Quantifying onset period rather than single date reveals projected intensification of dry-to-wet season transition.

Marcia T. Zilli, Jerry Samuel, Fran Morris, Neil C. G. Hart

School of Geography and the Environment, University of Oxford, Oxford OX1 3QY, UK

Marcia T Zilli

marcia.zilli@ouce.ox.ac.uk

https://orcid.org/0000-0003-1670-8567

27 August 2026

Quantifying onset period rather than single date reveals projected intensification of dry-to-wet season transition.

Marcia T. Zilli[1], Jerry Samuel[1], Fran Morris[1], Neil C. G. Hart[1]

[1] School of Geography and the Environment, University of Oxford, Oxford OX1 3QY, UK

E-mail: marcia.zilli@ouce.ox.ac.uk

Abstract.

Recent years have seen increasingly frequent delayed rainfall onset, especially in South America (SAm) and Southern Africa (SAfr). This arrival of the wet season is critical to water resources, ecosystems, and rain-fed agriculture. Existing rainfall-based approaches define the rainfall onset by a single date, limiting their ability to characterise the progression into the wet season. We introduce a novel method to identify the dry-to-wet transition period (DWTP) in rainfall time series, which better reflects this seasonal progression. The DWTP is defined as the interval between the first significant rainfall after the dry season and the establishment of sustained wet-season conditions. Identifying an onset period enables the quantification of key transition characteristics, including intensity, precipitation rate, dry day frequency, and duration. The method has the flexibility to be applied across regions, variable data resolutions, and different data sources.

Applied to observations, the method reproduces the observed spatial progression of the rainy season across both SAm and SAfr, with the first rains of the DWTP occurring 4-8 weeks before conventional rainfall accumulation onset dates. Our approach shows substantial regional variability in the intensity and duration of the transition into the wet season that is not captured by single-date metrics. The method captures widely reported onset delays in high-emission end-of-century scenarios, unambiguously showing later arrival of the first rains of the season across both regions. However, the method reveals these delayed first wet spells are likely to be followed by more intense and therefore abrupt establishment of wet seasons. These future changes are diagnosed in pioneering km-scale convection-permitting regional climate simulations over SAm and SAfr, with similar changes projected in the convection-parametrised driving global climate model and HadGEM3 CMIP6 projections. As risk of delayed rainfall onset grows, the DWTP framework may also have important potential applications in seasonal-to-subseasonal forecasting for early warnings.

Keywords: monsoon onset, dry-to-wet transition period, South America, Africa, convection-permitting models

Submitted to: *International Journal of Climatology*

1. Introduction

The start of wet season is a critical period in annual cycle of monsoonal hydro-climates. This start anchors the calendars of agriculture, water resources, and ecosystems. Recent years are increasingly being marked by pronounced variations in both timing and character of wet season onset in South America and Southern Africa. In Southern Africa, onset was delayed up to 30 days in austral spring of 2024 with prolonged early season dry spells and above average temperatures during December delaying planting in many countries (FEWS-NET 2025).

In South America, the 2023 dry season in the Amazon amplified one of the most severe regional droughts in recent decades (Stríkis et al. 2024). The extreme dryness and delay in wet season onset led to record-breaking temperatures in a series of spring heatwaves across Brazil (Espinoza et al. 2024, Marengo et al. 2024).

The onset of the rainy season can be identified using either regional circulation definitions or local rainfall definitions. Regional definitions have been applied to monsoons globally, including over South America where the start date of the rainy season is calculated based on changes in the regional thermodynamics and circulation patterns (e.g. Gan et al. 2004, 2005, Raia & Cavalcanti 2008) or as the main mode of variability based on a combination of variables (e.g. da Silva & Carvalho 2007, Jones & Carvalho 2013). In contrast, local onset definitions are typically based on accumulated precipitation thresholds (Janowiak & Xie 2003, Marengo et al. 2001) or other rainfall-related variables (e.g., soil moisture or longwave radiation; Horel et al. 1989, Kousky 1988). Local rainfall-only definitions are often defined precisely to inform specific sectors or decisions, such as crop planting dates. Such agronomic definitions are formulated based on field-scale thresholds such as X mm of rain over Y days not followed by a dry spell longer than Z days. These definitions are in wide operational use across Africa (e.g. Fitzpatrick et al. 2015, Mwangi et al. 2024, Reason et al. 2005). However, such hard thresholds rarely work well with gridded datasets, especially from climate models, due to both spatial averaging and convection rainfall from parametrised models often falling "too lightly, too often" (e.g. Garcia-Carreras et al. 2015). Application of such methods to climate models can lead to unclear identification of onset and contradictory findings in onset date changes (e.g. over southern Africa, Lawal et al. 2024).

To avoid threshold-sensitive local rainfall onset definitions, many climate studies focused on timing of rainfall onset (e.g. Bombardi & Boos 2021, Dunning et al. 2018) have adapted the accumulated rainfall anomaly metric for onset date (Liebmann et al. 2012, Liebmann & Marengo 2001). The daily rainfall anomaly is defined with respect to annual daily mean rainfall. Onset is identified by the turning point in a curve computed by accumulating the daily anomaly from a date within the dry season. When daily rainfall starts exceeding the annual daily mean this accumulation curve will turn from accumulating an anomalous daily rainfall deficit to a surplus. In practice, this curve is often smoothed and then the turning point is defined as onset date (Bombardi et al. 2019). This is a well-posed approach to capture onset across a range of climates of varied rainfall intensities and across a range of observational and model data sources. This success comes because the daily anomaly is adaptive to different rainfall distributions in different data sets and, as demonstrated in Mwangi et al. (2024), overcomes the challenges introduced by the absolute thresholds necessary for agronomic definitions.

This accumulated anomaly method has been central to diagnosing observed and projected delays in onset, particularly, across South America and southern Africa. Both regions have high CMIP intermodel agreement with a projected spring (September-November) rainfall decline (e.g. Chadwick et al. 2025, Munday et al. 2025), which has been shown to result in onset date delays of 2-4 weeks (Bombardi & Boos 2021, Dunning et al. 2018). However, these previous studies have only provided information about timing and not other characteristics of the onset.

In reality, the arrival of the wet season is not a date but a transition, which is mediated by thermodynamic changes, land-surface and vegetation feedbacks, and large-scale circulation responses (Fu et al. 1999, Li & Fu 2004). Naturally, there are large regional and interannual differences in the character of this transition, which are also affected by climate change. For example, Samuel et al. (2025) showed how projections of end-of-century climate over Eastern Brazil indicate that the extension of the dry season (already documented in observations, Fu et al. 2013) is followed by a substantially more abrupt transition into the wet season than seen in the contemporary climate. Therefore, a local rainfall-based approach is required, which captures the *transition* from dry to wet seasons.

This paper introduces a novel methodology to bridge this gap between the methods considering (thermo-)dynamics of season transitions and single-date local rainfall onset. The method is applied to local (grid-scale) rainfall time series to diagnose the period during which the transition from the dry to the wet season occurs. We use the method to quantify future changes to the timing and characteristics of this transition. By considering an onset period rather than a single date, we can quantify the future changes in the *characteristics* of the transition into the wet season, such as intensity, duration, or frequency of dry days.

Furthermore, we present the first assessment of these onset changes in large-domain regional convection-permitting simulations for southern Africa (SAfr, hereafter) and SAm (SAm, hereafter). These simulations are particularly worth consideration for monsoon season transitions due to the highly convective nature of this rainfall and the widely reported improvements in the rainfall spectrum simulated by convection-permitting models (CPMs). Relevant improvements include higher fractions of dry days and better representation of intense rainfall (Halladay et al. 2023, Kendon et al. 2017, Lenderink et al. 2024). These CPM gains are particularly evident over SAm and Africa (Kendon et al. 2019, Zilli et al. 2024). Over SAfr especially, the CPM simulates a 50% lower mean-state wet bias in summer rainfall than the driving GCM due to enhanced large-scale subsidence (Hart et al. 2018). This wet bias is typical of CMIP model simulations and this improvement delivers better representation of the SAfr annual cycle (Hart et al. 2018).

The DWTP framework and the data used to characterise it are described in Section 2. The climatology of the present-day DWTP is described in Section 3, while future projections are presented in Section 4. Section 5 discusses the main results with Conclusions presented in Section 6.

2. Data and Methods

2.1. Data

To analyse the dry-to-wet-transition period (DWTP) in Southern Africa (SAfr) and South America (SAm), we considered daily precipitation data from the Climate Hazards Center Infrared Precipitation with Station data (CHIRPS; Funk et al. 2015), a gridded rainfall product obtained by merging satellite imagery and in-situ station data. Similar results were also obtained using precipitation from the fifth generation reanalysis (ERA5) of the European Centre for Medium-Range Weather Forecasts (ECMWF; Hersbach et al. 2020).

For historical simulations and future climate projections, we use a suite of convection-permitting regional climate model (CPM) and parametrised convection simulations produced by the UK Met Office (UKMO). Both present and future scenarios have 10 years of simulation each over tropical and subtropical SAm (85° – 30°W, 40°S – 15°N) and Africa (25°W – 56°E, 39°N – 45°S), although here we focus only on the southern portion of this domain (10°E – 55°E, 0° – 45°S). The CPM simulations use the Met Office Unified Model (UM) with horizontal grid spacing of 4.5 km, in which the deep convection parametrisation is turned off. The present-day CPM scenario (CPM-PD) covers the 1997-2006 (SAfr) and 1998-2007 (SAm) period and is obtained by directly nesting it in the UKMO atmosphere-only global climate model (MOHC-HadGEM3-GA7GL7, GCM-PD hereafter) run at 25 km horizontal grid spacing (N512L85 Gaussian grid). For a detailed description of the UKMO CPM configuration and the present-day simulation over SAfr, see Stratton et al. (2018); for simulations over SAm, see Halladay et al. (2023).

The future GCM scenario (GCM-FUT) is obtained by running the GCM using greenhouse gases levels from the CMIP5 RCP8.5 protocol, with fixed CO_2 concentration (936 ppm) and future sea surface temperatures (SSTs) for a 10-year period around 2100. The future SSTs are obtained by adding the monthly SST changes between the present (1975–2005) and future (2085–2115) scenarios from HadGEM2-ES RCP 8.5 simulations to the present-day daily SST dataset (Reynolds et al. 2007). The GCM-FUT is then used to drive the CPM, resulting in 10 years of the convection-permitting future simulation (CPM-FUT). More details on the configuration of the future simulations are available in Kendon et al. (2019), for SAfr, and Kahana et al. (2024), for SAm.

Results for the CPM are also compared with the simulations from UKMO HadGEM3-GC3.1 (Williams et al. 2018) historical and future (ssp585) scenarios, in two spatial resolutions: N216 Gaussian grid (Andrews et al. 2020), which equates to a nominal atmospheric resolution of $\sim$60 km; and N96 (Kuhlbrodt et al. 2018), with nominal atmospheric resolution of $\sim$135 km, available in the Coupled Model

Intercomparison Project 6 (CMIP6). While resolution (ranging from 135 *km* in N96 to 4.5 *km* in the CPMs) and science settings differ between configurations (regional versus global), all simulations share the same UM version (Version 10.6).

2.2. Dry-to-Wet Transition Period (DWTP) definition

The objective of the DWTP algorithm is to identify the period from the first rains that end the dry season to the wet season being clearly established. The method uses filtered daily precipitation and its rate of change and is applied in two steps: identify the broad climatological timing of the DWTP, referred to as the climatological envelope, followed by a refinement of the DWTP in each year. Here, we demonstrate the use of the method over regions with one rainy season. However, the method is flexible to identify regimes with two (or more) rainy periods.

2.2.1. DWTP Climatological Envelope The first step identifies the climatological timing of the DWTP at each grid point as the period of sustained increase in precipitation after the dry season. The process is illustrated in Fig. 1. We start by filtering daily precipitation (grey lines in Fig. 1a) using a low-pass second-order 60-point Butterworth Filter to obtain the primary signal of increasing seasonal rainfall. Varying the filter window width in the range from 30 to 90 days produces only minor changes to the timing. The choice of a Butterworth filter avoids numerical artifacts ("ripples") produced by the Fast Fourier Transform during zero precipitation periods. The Butterworth-filtered precipitation (PR_{60}) is represented by the thick black line in Fig. 1a. We then proceed to calculate the gradient of the PR_{60} (dPR_{60}/dt, red line in Fig. 1a, multiplied by 100 for plotting on same axis) and identify periods in which both the PR_{60} and dPR_{60}/dt are positive for more than 30 consecutive days (green areas in Fig. 1a). This 30-day criterion ensures that the selected periods correspond to periods with sustained increase in precipitation and removes short-lived wet spells (see red area in the beginning of 2001 in Fig. 1a, for example).

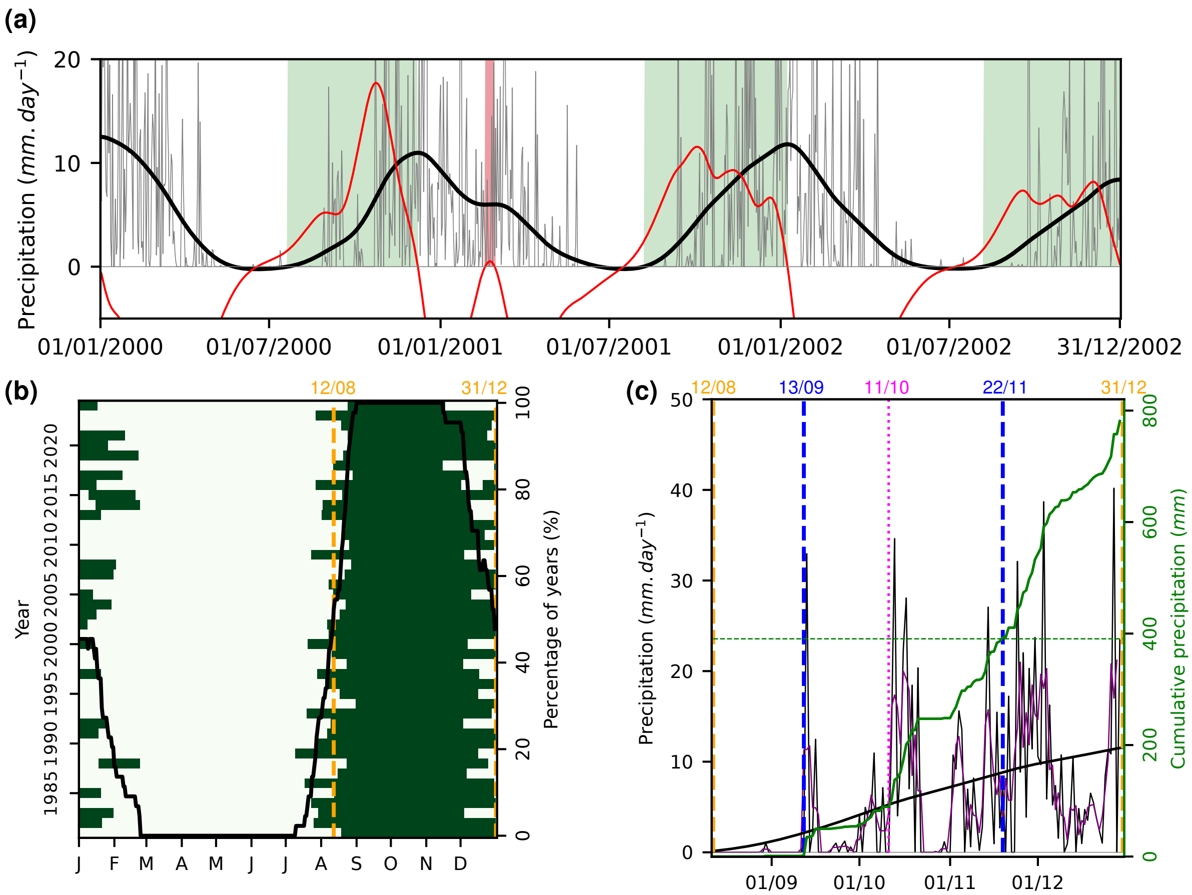

Figure 1. Graphics exemplifying the DWTP framework, using the observed (CHIRPS) precipitation at 15°S, 50°W. (a) Daily precipitation rate between 01/Jan/2000 and 31/Dec/2002 (in $mm.day^{-1}$, thin grey line), its filtered values (PR_{60}, in $mm.day^{-1}$, thick black line) and its gradient (in $\times 10^{-2} mm.day^{-2}$, red line). Areas where both PR_{60} and its gradient are positive are shaded in green (longer than 30 days) and red (less than 30 days). (b) Days with positive PR_{60} and its gradient in each year (green bars) and percentage of years in which these time series were positive in each day of the year (black line in reference to secondary y-axis). Vertical dashed orange lines indicate the climatological envelope. (c) Daily precipitation during the climatological envelope of 2001 (12/Aug to 31/Dec, in $mm.day^{-1}$, thin gray lines) and its 3-day running mean ($mm.day^{-1}$, thin purple line), the PR_{60} ($mm.day^{-1}$, thick black line), the first and last day of the DWTP (dashed blue lines), and the onset date (magenta dotted line). The green line represents the cumulative precipitation (in mm on secondary y-axis) and the horizontal dashed green line marks the 50% of cumulative precipitation at the end of the climatological envelope for 2001.

This step is applied to the entire multi-year time series, identifying periods with positive PR_{60} and its gradient in each year (green bars in Fig. 1b). We then calculate the percentage of years with positive values for both of these attributes on each day of the year (represented by the black line in Fig. 1b). The climatological envelope is defined as the period in which both PR_{60} and dPR_{60}/dt are positive in more than 50% of the years (dashed orange lines in Fig. 1b). The process is straightforward in regions with a single well-behaved rainy season, such as the one represented in Fig. 1b, but requires a further set of rules in regions with two rainy seasons.

2.2.2. Year-to-Year Refinement The second step of the methodology sharpens the start and end of the DWTP in each year, as illustrated for a location over South America in the austral spring of 2001 (Fig. 1c). Starting from the climatological envelope (delimited by the dashed orange lines in Fig. 1c), we refine the start of the DWTP in a given year as the first day with significant precipitation after the longest dry spell within the climatological envelope. Here, we use a 3-day running mean filtered precipitation (thin purple line in Fig. 1c) to smooth small variations. Significant precipitation is defined as any 3-day filtered precipitation with values above 10% of the maximum PR_{60} within the climatological envelope of that year. For the example in Fig. 1c, this would be any daily precipitation above 1.2 $mm.day^{-1}$, equivalent to 10% of the maximum value of the thick black line in 2001-2002 during the climatological envelope (between yellow dashed lines). By using a threshold based on the smoothed precipitation (PR_{60}), we take into account the climatology of the region and the variability of that year when defining a "significant rain", with smaller values triggering the first day in drier regions or in years with below-average precipitation. This relative threshold also allows straightforward application to raw precipitation from climate and seasonal forecast systems, without the need for bias-correction.

By defining the first day of the DWTP as the first substantial rains after the longest dry spell, we also account for the possibility of dry spells or breaks in the DWTP. In this illustrative year (2001), a minor rain spell occurred at the end of August, but did not reach the significant threshold (Fig. 1c). Thus, this event does not interrupt the lack of substantial rainfall during the first 31 days of the climatological envelope in this year, which are therefore considered as a dry spell. Since this is the longest dry spell in this year, the first day of the DWTP is 13^{th} September (first blue dashed line in Fig. 1c). There are other dry spells in this season (for example, in the beginning of November), but they are shorter than the one at the beginning of the climatological envelope.

The end of the transition into the wet season is a less physical concept than the first rains in that it only needs to indicate when the wet season has become well-established in a given year. Here, this is simply chosen to be when the cumulative precipitation (green line in Fig. 1c) reaches 50% of the total within the climatological envelope for that year (dashed green line in Fig. 1c). In this example, the end of the DWTP occurs on 22^{nd} November (second blue dashed line in Fig. 1c).

This refinement is repeated for each year and grid point. In regions with multiple rainy seasons and, consequently, multiple climatological envelopes, the process is repeatedly applied for each climatological envelope separately. The final output of the method is the DWTP, defined by the first day and duration, computed at each grid point and for each year.

This dependence of the end date on cumulative precipitation within a given year means that *duration* of the DWTP is dependent on early season rainfall intensity. However, to explicitly quantify the general intensity of start of the wet season, *onset intensity* is computed as the mean gradient of the PR_{60} within the DWTP. A range of additional metrics can be computed within the DTWP. Here we include fraction of dry days ($< 1mm.day^{-1}$) and average precipitation rate of the period.

2.2.3. Onset Date While the DWTP method computes at least four characteristics to describe the onset of a rainy season, it is worth including a comparison to well-established methods that compute a single onset date. Here we do so using the cumulative daily precipitation anomaly, first described by Liebmann & Marengo (2001) and widely applied by others (Bombardi et al. 2019, Dunning et al. 2016). For full details on the identification of the rainy season onset date, refer to Bombardi et al. (2019). In brief, this method defines the rainy season onset date as the inflexion point of the cumulative daily precipitation anomaly time series (S), given by:

$$S(n) = \sum_{i=t_0}^{n} (P_i - P_m) \tag{1}$$

where, P_i is the daily precipitation rate for the i^{th} day and P_m is the long-term mean annual precipitation rate (both in $mm.day^{-1}$). t_0 is the starting date of the water year and is chosen as the minimum of the first harmonic of the climatological annual cycle of daily rainfall, marking the climatological peak of the dry season. The precipitation anomalies are accumulated from this day moving forwards in the water year, resulting in negative values during the dry season. As daily rainfall increases, the cumulative curve reaches a minimum and starts to increase, in general. The date corresponding to this minimum is identified as the onset date of the rainy season. However, for a very gentle evolution of rainfall, an inflexion point may not be appropriate to define the onset and an additional step is performed. In such cases, the onset date is defined as the first day when the derivative of the smoothed S curve changes sign and persists for 3 days. In Fig. 1c, the onset date is represented by the dashed magenta line. As seen in Fig. 1c, this onset date typically occurs within the DWTP.

3. Climatology of the DWTP

3.1. Timing

Much of SAm and SAfr is characterised by the presence of one rainy season during austral summer. In most of SAfr, the onset date, as estimated using Bombardi et al. (2019) methodology (Eq. 1), occurs after September (Fig. 2a). Exceptions are found over the arid west coast, where the onset date is in January or during the austral autumn for the winter rainfall region in the southwest. Note that climatological dates are calculated using the circular median to manage variability in dates which may fall across calendar years. The rainy season onset occurs first in the Congo Basin and eastern South Africa in early September. As the season progresses, the rains reach areas over central SAfr in late October/early November, finally reaching the east coast of Mozambique and Madagascar in December. This pattern is well-described in literature (e.g. Dunning et al. 2016, Liebmann et al. 2012, Tadross et al. 2005).

This progression is also depicted on the transect (see dashed red box in Fig. 2) across the region with the largest spatial gradient in the onset date (dashed blue line in Fig. 3a). The first day of the DWTP follows a similar progression to the onset date but occurs 3-6 weeks earlier, depending on location (Fig. 2c and solid blue line in Fig. 3a). This lag between the first day of the DWTP and the onset date is expected, since by definition the DWTP starts with the first rains of the season and, consequently, before the accumulated rainfall onset date. In fact, the onset date occurs within the DWTP 85% of the time over SAfr; in most of the remaining cases the onset date is after the end of DWTP, mainly over the more arid parts of western and southwestern South Africa, where rainfall is infrequent (not shown). The spatial progression of the DWTP is consistent across years, with indications of interannual variability (shades in Fig. 3a). The DWTP lasts between 60 and 110 days in most of the regions (Fig. 2e), with longer

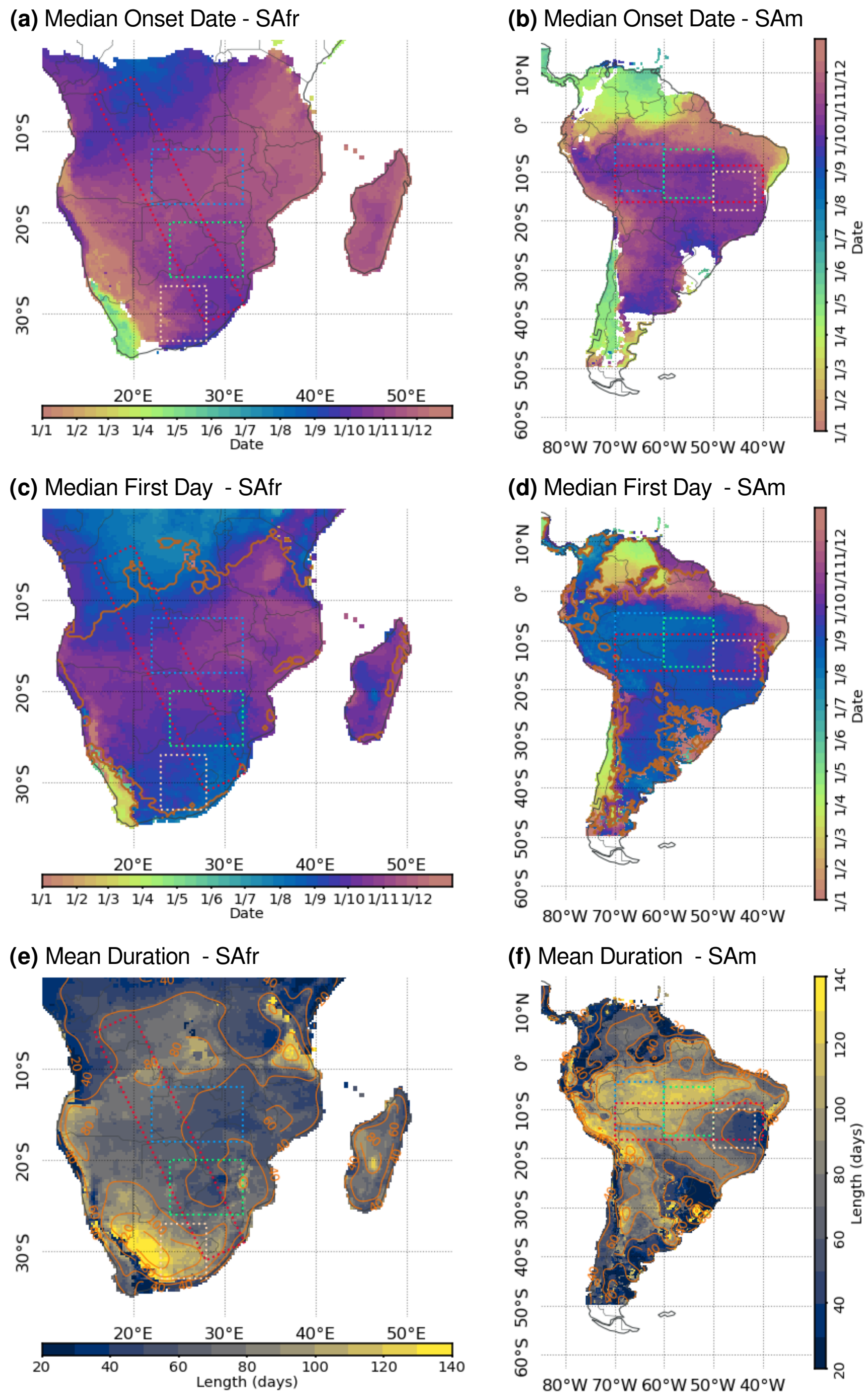

Figure 2. Main characteristics of the DWTP in Southern Africa (left) and South America (right), considering observed precipitation (CHIRPS). (a), (b) Median onset date, (c), (d) Median first day of the DWTP, with orange contour delimiting areas with one DWTP. (e), (f) Mean duration of the DWTP (contours each 20 days). In all maps, the dashed boxes indicate the study regions. For SAfr (left): Zambia (ZBS, dashed blue), the Limpopo Valley (LPP, dashed green), East Cape province in South Africa (SAf, dashed light yellow), and a transect (dashed red). For SAm (right): west Amazon (WAmz, dashed blue), east Amazon (EAmz, dashed green), eastern Brazil (EBr, dashed light yellow), and a transect over the core of the monsoon region (dashed red).

DWTP over parts of southwestern SAfr, where it can last more than 120 days, again related to highly episodic rainfall and therefore only gradual accumulations across a season.

The first day of the DWTP (shading) across the 10-year present day CPM simulation over SAfr (CPM-PD) is shifted only 1-2 weeks earlier than observations, especially around 15-20^{o}S where colours are more blue than purple (Fig. 3c).

In tropical SAm, the onset date occurs between late September and late November (Fig. 2b), in line with the west to east progression of the South American Monsoon System (dashed blue line in Fig. 3b; see red box in Fig. 2b for the location of the transect). Over the subtropics (south of ∼20°S), the onset date is slightly earlier, progressing towards the core of the monsoon region. The onset date is in April/May over northern SAm, related to the migration of the monsoon system back towards the northern hemisphere. In south Chile, April onset of the winter rainfall season is also diagnosed, related to the equatorward shift of the storm track in the austral autumn/winter (Garreaud 2013). Over the northern and northeastern Brazilian coast, the onset date occurs in late December/early January, following the ITCZ progression. Similar patterns are described in Bombardi & Carvalho (2009), Marengo et al. (2001), Raia & Cavalcanti (2008).

As in SAfr, the first day of the DWTP in SAm follows a spatial pattern similar to the onset date (Fig. 2b), with the onset date occurring within the DWTP 75% of the time. The onset date is typically only after the end of DWTP where the rainy season is not well defined, such as over Northeast and South Brazil. Over the Amazon region, the lag between the first day of the DWTP and the onset date is larger, revealing a more gradual transition from the dry to the wet season (solid blue line in Fig. 3b). There is a clear west-to-east progression of the start of the transition season captured by the

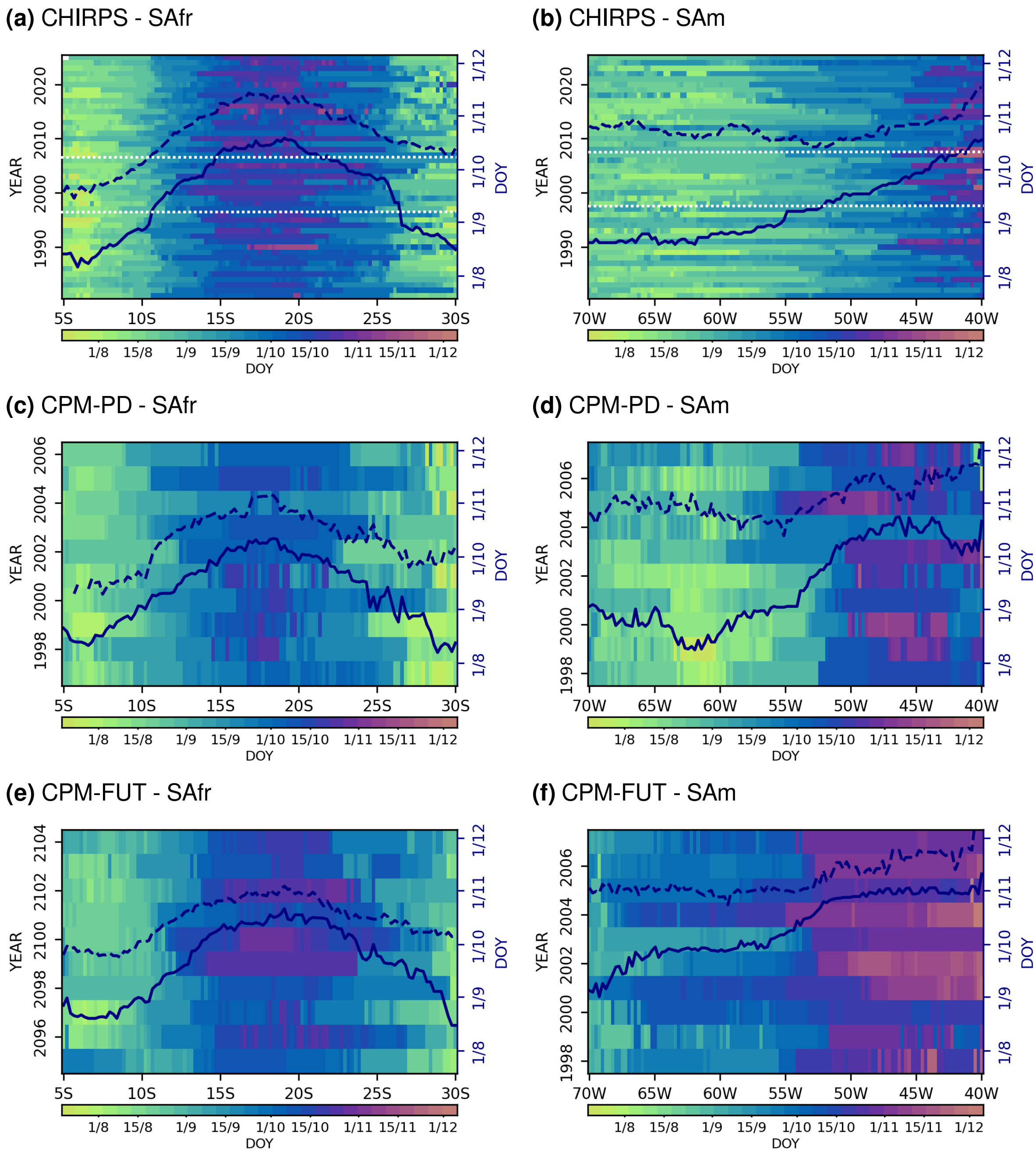

Figure 3. Median first day of the DWTP for each year (shades) and median over all years (secondary y-axis) for the first day of the DWTP (solid blue line) and the onset date (dashed blue line), averaged over the transects over SAfr (left) and SAm (right). See red dashed areas in Fig. 2 for the location of the transects. Latitudes (longitudes) in the graphics refer to the transects' major axis. Datasets are: (a), (b) CHIRPS; (c) CPM-PD over SAfr; (d) CPM-PD over SAm, (e) CPM-FUT over SAfr, and (f) CPM-FUT over SAm. The dotted white lines in (a), (b) indicate the period of the simulations in (c) to (f).

first day of the DWTP (solid blue line, Fig. 3b), which is not seen when considering the onset date (dashed blue line).

The SAm CPM-PD simulation captures this eastward progression of the first day; however the earlier median start in the central Amazon (~60^{o}W, solid blue line, Fig. 3d) and later arrival in eastern Brazil amplify the strength of this progression. In general, the CPM-PD first days (shading) are 2-4 weeks late relative to observations.

3.2. Precipitation rate, fraction of dry days, and intensity

By defining the transition into the wet season as a period, we can estimate other attributes derived from daily precipitation, such as the precipitation rate, frequency of dry days, and overall onset intensity. We can also derive properties associated with other variables and metrics during the transition season, such as the mean soil moisture increase (a measurement of the DWTP efficiency) and the number and type of key rainfall systems supporting onset. Here, we demonstrate this characterisation using mean precipitation rate, fraction of dry days, and onset intensity.

In both study regions, the DWTP is related to the establishing monsoon regime, and this is reflected in the spatial distribution of the mean precipitation rate and fraction of dry days ($< 1\ mm.day^{-1}$) during the DWTP (Fig. 4). In SAfr, the highest precipitation rates during the DWTP are observed in the Congo basin, Zambia, Malawi, south Tanzania, north Mozambique, and Madagascar, with values above 4 $mm.day^{-1}$ on average (Fig. 4a). This area also has the lowest fraction of dry days during the DWTP, with values below 60% (Fig. 4c). In the southern part of SAfr, the DWTP is characterised by lower average precipitation rates ($<$2 $mm.day^{-1}$) and larger fraction of dry days (~70% or more).

In SAm, the DWTP is generally wetter than in SAfr, with the largest averaged precipitation rates observed in the Amazon (~5 $mm.day^{-1}$), parts of central and eastern Brazil along the climatological position of the SACZ (Carvalho et al. 2004, Kodama 1992), and over subtropical SAm (Fig. 4b), in the region with frequent mesoscale

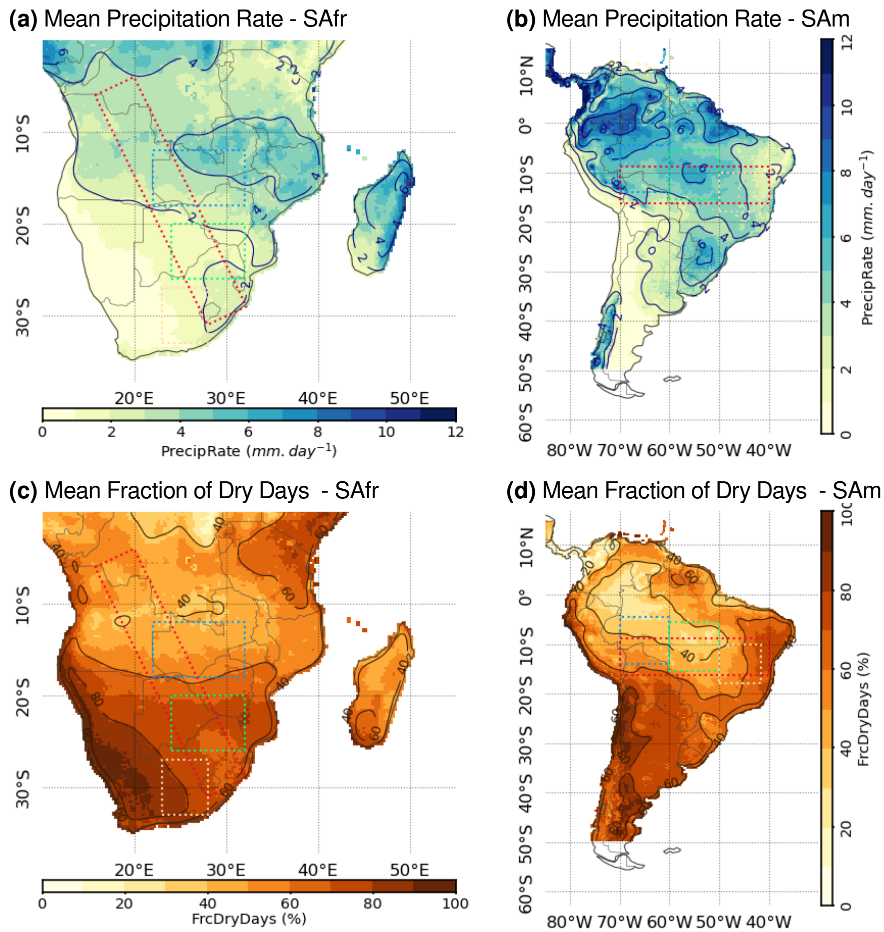

Figure 4. Characteristics of the DWTP in SAfr (left) and SAm (right), considering the observed precipitation (CHIRPS). (a) and (b) Mean precipitation rate (in $mm.day^{-1}$, contours each 2 $mm.day^{-1}$);(c) and (d) Mean fraction of dry days (in %, contours each 20%). In all maps, the dashed boxes indicate the study regions. For SAfr (left): Zambia (ZBS, blue), Limpopo Valley (LPP, green), South Africa (SAf, light yellow), and a transect (dashed red). For SAm (right): west Amazon (WAmz, blue), east Amazon (EAmz, green), eastern Brazil (EBr, light yellow), and a transect over the core of the monsoon region (dashed red).

convective system activity (Gilmour et al. 2025, Mattingly & Mote 2017). The fraction of dry days is also smaller over these regions (Fig. 4d), with values below 40% in the Amazon. The driest DWTP occurs in northeastern Brazil and southern SAm, where the mean precipitation rate is below 2 $mm.day^{-1}$ and with more than 70% of dry days.

We also consider a third characteristic of the DWTP, the onset intensity, defined as the mean gradient of smoothed precipitation, PR_{60}, during the DWTP, effectively quantifying the intensity with which the wet season is established. Over Western

Amazon (WAmz, dashed blue box in Fig. 2 right), for example, PR_{60} increases gradually from the lower rain rates of mid-July until the peak of the rainy season in mid-February (see blue line in Fig. 5a). This gradual increase results in a 3.5-month long DWTP, with the onset date occurring towards the end of the DWTP (orange triangle and dashes in Fig. 5a) and an onset intensity of $\sim$0.06 $mm.day^{-2}$ (shades in Fig. 5a). The process is similar in Eastern Amazon (EAmz, dashed green box in Fig. 2 right) with the DWTP starting a couple of weeks later than WAmz and with a shorter 3-month duration (Fig. 5b), resulting from slightly more intense onset ($\sim$0.08 $mm.day^{-2}$). In contrast, Eastern Brazil (EBr, dashed light yellow box in Fig. 2 right), which has a 3-month long dry season with near-zero rainfall, sees an increase in PR_{60} from the end of August and reaches its peak by the middle of December (blue line in Fig. 5c) with greater onset intensity ($\sim$0.09 $mm.day^{-2}$, shading in Fig. 5c). This greater intensity also results in a shorter duration DTWP than the Amazon regions. Nieto-Ferreira & Rickenbach (2011) identified a similar behaviour, with abrupt onset in Eastern Brazil related to synoptic activity in the region of the SACZ.

The SAm CPM-PD simulation captures this regionally-averaged onset intensity well (Fig. 5d-f). However, there is $\sim$2-week delay in the simulated DWTP first day in EAmz and greater onset intensity (Fig. 5e).

Over SAfr, three subregions are chosen (boxes in Fig. 2a). The Zambia box (ZBS) sits within the core of the African rain belt during the wet season (e.g. Fig. 2 in Hart et al. 2019). The Limpopo River Valley (LPP) box covers a well-documented drought corridor with high onset variability and dry spell risk (e.g. Tadross et al. 2005, Thoithi et al. 2021). The South Africa box (SAf) is located across the highly variable western margin of the subtropical convergence zone which is strongly dependent on tropical-extratropical cloud band rainfall (Hart et al. 2013). Fig. 6 (a-c) shows how the onset

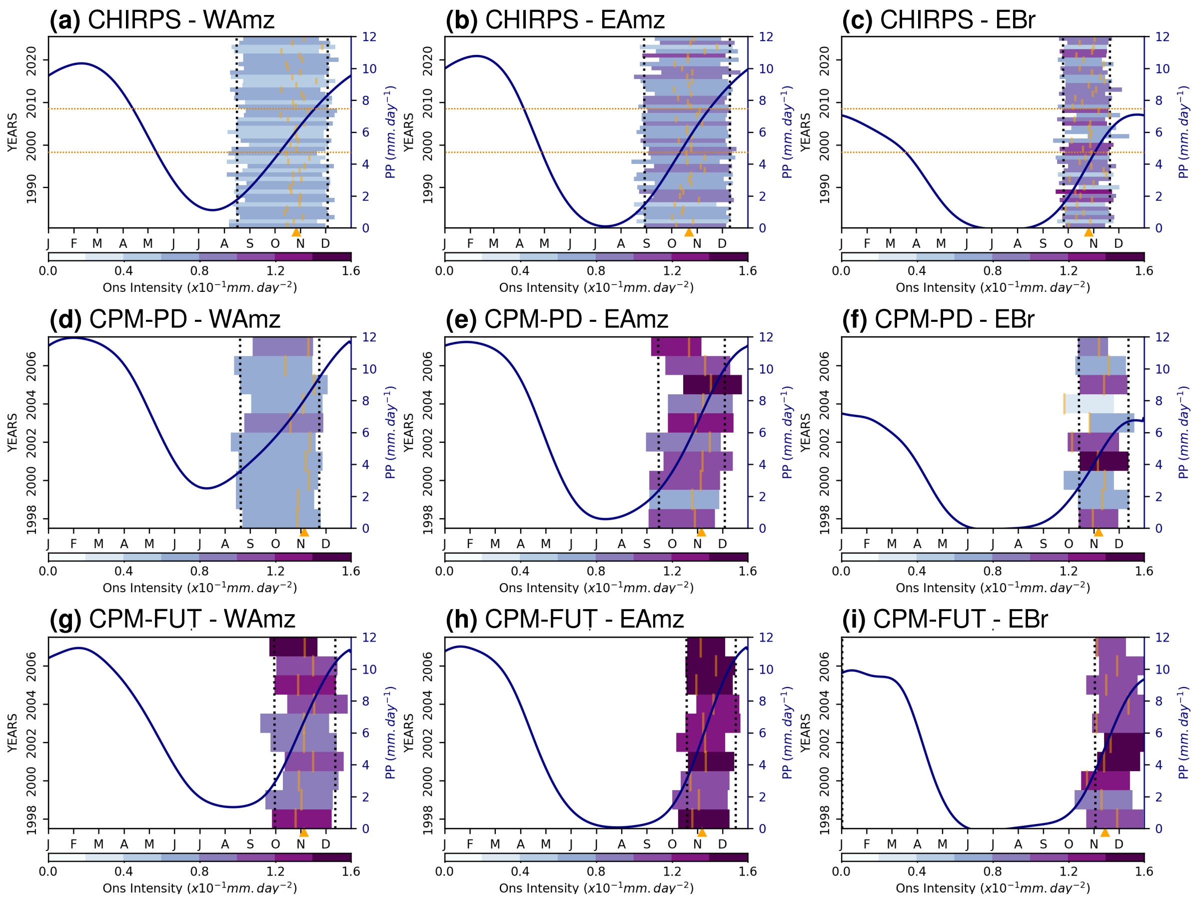

Figure 5. Annual cycle of the Butterworth-filtered precipitation (PR_{60}, in $mm.day^{-1}$, blue line) and the area-averaged onset intensity per year within the DWTP (shades in $\times10^{-1}mm.day^{-2}$) considering data from: (a)-(c) CHIRPS observations; (d)-(f) CPM-PD; and (g)-(i) CPM-FUT. In each graphic, the vertical dotted lines indicate the median DWTP, the orange triangle by the x-axis indicate the median onset date for the area, and the orange dashed lines indicate the area median onset date per year. The dotted yellow lines in (a)-(c) indicate the period of the simulations in (d) to (i). Graphics are for (left) Western Amazon (WAmz), (middle) Eastern Amazon (EAmz), and (right) Eastern Brazil (EBr). See Fig. 2 (right) for the location of these areas.

intensity decreases polewards across the continent. This decrease is associated with lower peaks in wet season rainfall rates as you move from the tropics (ZBS) into the subtropics (SAf) and longer transitions into the wet season.

Generally, the CPM-PD simulation over SAfr reproduces the timing of the observed first day and onset date to within a week of the observations for each area average, although magnitude of the peak seasonal precipitation rate, PR_{60}, is 1-2mm/day wetter than observed.

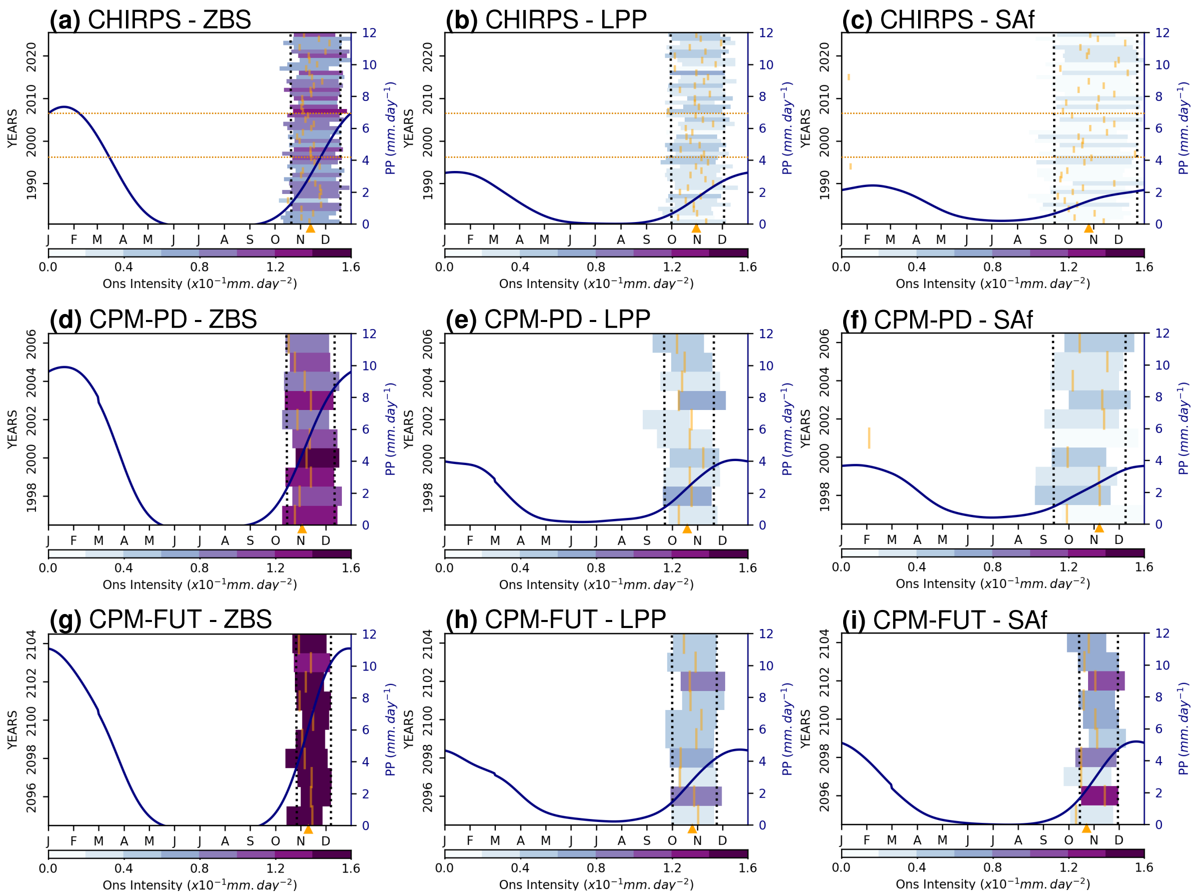

Figure 6. As in Fig. 5 but for areas over SAfr: (left) Zambia (ZBS), (middle) Limpopo Valley (LPP); and (right) South Africa (SAf). See Fig. 2 (left) for the location of these areas.

4. Future Changes in dry-to-wet season transitions

Across both SAm and SAfr, the high emissions scenario simulated in CPM-FUT shows the widely reported projection for delays in the onset date (blue dashed lines Fig. 3e-f) (Bombardi & Boos 2021, Dunning et al. 2018). Since this onset date is computed from accumulation of daily rainfall anomalies, there is some ambiguity whether these delays represent a true extension of the dry seasons or capture lower early season rainfall rates and therefore a later turning point in anomaly accumulation leading to a later onset date. Similar delays of 2-4 weeks in the first day of the DWTP introduced in this paper, indicate these delays are indeed in the first rains of the season too confirming the extension of the dry season (solid blue line, Fig. 3e-f). The 2-4 week delays are seen in both the climatological median days (blue lines, Fig. 3e-f) and in the shading which moves from green to blues and blues to purples across most of the years in the 10-year end-of-century time slice.

The annual cycles represented in Figs. 5g-i and 6g-i further detail these changes. In all areas, the future dry season is longer. In WAmz and EAmz, where the dry season rains a little in present climates, the future is drier (see blue line representing PR_{60}). In WAmz and EAmz, the first day of the DWTP occurs $\sim$ 30 days later in the CPM-FUT compared to the CPM-PD; in SAfr, the DWTP starts $\sim$ 10 days later (see also shades in Fig. 3c-f). The transition period also contracts reflecting that rainfall accumulates more quickly across the dry-to-wet transition. This contraction is expected from the higher onset intensities across these regions (shades in Figs. 5g-i and 6g-i).

These CPM-projected increases in onset intensity suggest that the delayed rains across SAm and SAfr may be followed by more rapid establishment of the wet season. The delayed timing of the DWTP is also seen in the 25km parametrised-convection GCM which drives the regional CPMs and in the HadGEM3 CMIP6 model simulations (Fig. 7). However, the CPM projections generally indicate greater delays and intensification than the parametrised models.

The DWTP also enables analysis of changes in daily precipitation rates and fraction of dry days during the transition from the dry to the wet season (Fig. 8). As expected from established rainfall responses to warming, the mean precipitation rates during the DWTP increase in the CPM-FUT simulations and the CMIP6 models (Fig. 8a and b). This magnitude of increase varies by region and model, with the CPM-FUT not showing distinctly greater increases as may have been expected from other studies focused on the core of wet seasons (Kendon et al. 2019). The CPM does, however, produce higher fraction of dry days relative to the convection-parametrised models, which is in good

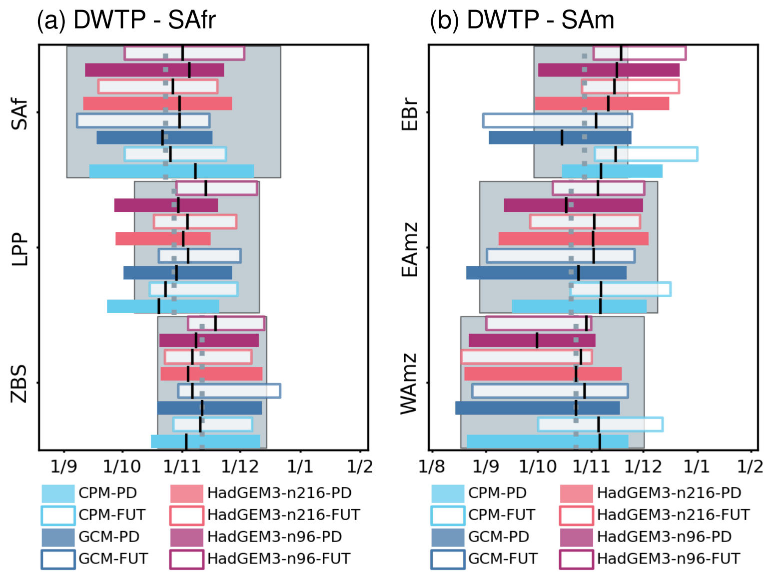

Figure 7. Timing of the DWTP over (a) SAfr and (b) SAm in observations (grey boxes) and simulations (bars; see colour key in the graphics) for all subregions (y-axis labels). The onset date in observations (dashed grey line) and models (black lines) are shown. Solid (empty) bars represent present-day (future) simulations. The dates are climatological medians. See Fig. 2 for name and location of each area.

agreement with observations over SAfr but too high over SAm. Decreases in fraction of dry days during the transition are projected for SAfr, especially for ZBS and LPP. These decreases are also seen in SAm, but only over EBr. This result suggests that especially in drier tropical regions (SAfr-LPP and SAm-EBr) the delayed and intensified transition to the wet season will also have fewer dry days than in present climate.

5. Discussion

This paper expands the identification of rainfall onset from a single date to a dry-to-wet transition period (DWTP), which starts with the first significant rains after the dry season and ends when the wet season is established. This approach provides a methodology more appropriate to established physical understanding of the transition into the wet season (e.g. Fu et al. 1999). The DWTP framework provides a breadth of information that is not readily available when considering a single date as the

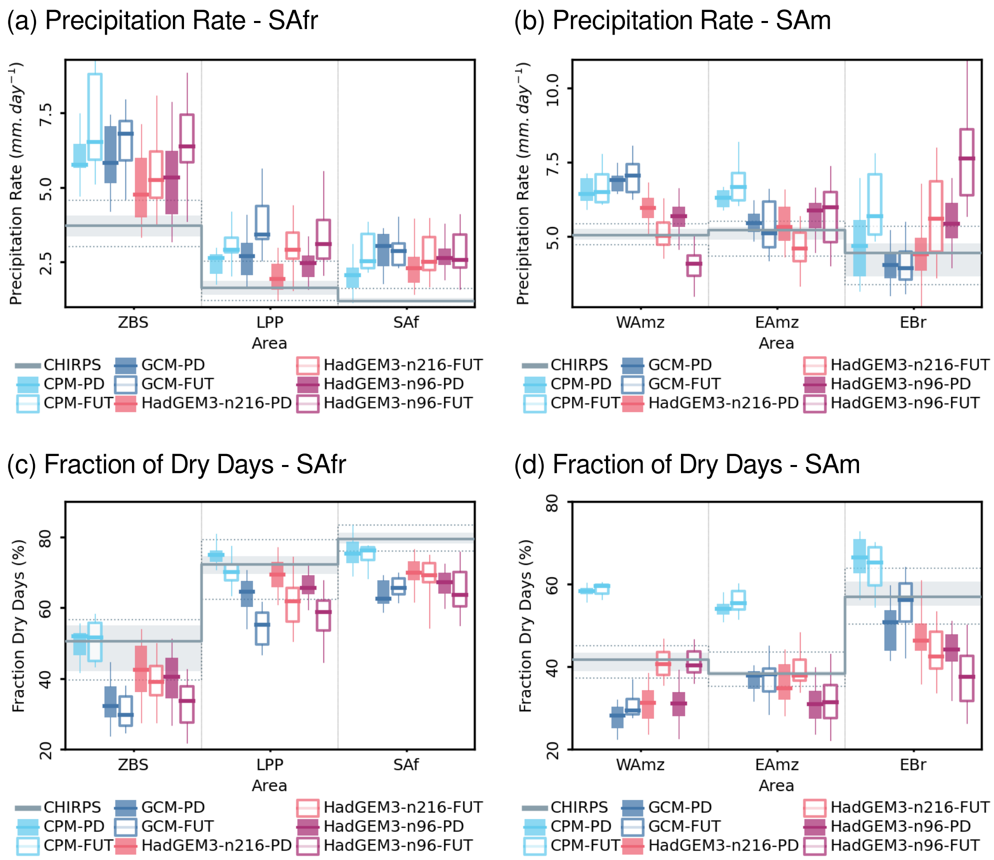

Figure 8. Characteristics of the DWTP in SAfr (left) and SAm (right): (a), (b) mean precipitation rate (in $mm.day^{-1}$) and (c), (d) mean fraction of dry days (in %), considering observations (grey lines and shaded envelope), and the simulations (box and whiskers) for present day and future scenarios, according to the colour key in the graphics. The box plots (and shaded envelope) indicate the interquartile range for each characteristic, considering the mean of the simulations (observations) over each area (see Fig. 2 for name and location of each area); the thick solid line indicates the median and the whiskers (and thin grey dotted line) the 5^{th} and 95^{th} percentiles. Note that the vertical scale of the graphics are different for the two continents due to high rain rates over SAm.

onset. Furthermore, the adaptative time series analysis which uses relative, rather than absolute, rainfall thresholds provides substantial flexibility for application to different data sources, grid resolution, area-averages, and climate regions. It is this flexibility which has enabled the analysis in this paper across observations and model simulations with horizontal resolutions ranging from kilometres to hundreds of kilometres.

The results presented here demonstrate the advantages of using this period-based analysis to complement the traditional evaluation of the onset date. The DWTP method captures the previously reported delays in rainfall onset across South America and southern Africa under continued planetary warming (Bombardi & Boos 2021, Carvalho & Cavalcanti 2016, Dunning et al. 2018). However, the method explicitly confirms that this is due to a delayed arrival of first wet spells of the season, rather than weaker early season rainfall slowing accumulation rates. Therefore, dry seasons are definitively projected to lengthen across SAm and SAfr. Furthermore, the DWTP diagnoses more intense and frequent (fewer dry days) precipitation, resulting in a more abrupt transition from the dry to the wet season. While there are region specific variations in magnitude of precipitation intensity and dry day changes, this abruptness of onset, quantified by the DWTP onset intensity metric and reflected in shorter DWTP durations, is seen across regions over South America and southern Africa. This projected abrupt dry-to-wet season transition was identified in Samuel et al. (2025) over central and eastern Brazil and aligns with the enhanced seasonality reported for projections of the Western Amazon using the same convection-permitting projections considered here (Kahana et al. 2024).

The mechanisms driving the delayed onset projected over southern African and South America remain under investigation (e.g. Chadwick et al. 2025). However, a series of papers diagnosing the moist thermodynamics of the delayed onset in these southern monsoons offer some explanation for the intensification of the dry-to-wet transition we have diagnosed. On regional scales, the differential warming along the atmospheric column will lead to increased stability (Bony et al. 2006), which increases the amount of near surface moist static energy (MSE) necessary to destabilise the air column and trigger convection. Bombardi & Boos (2021) showed that this increased demand for greater low-level MSE is not met over the South American or southern African monsoons, with both regions projected to develop MSE deficits relative to the increasing tropical mean MSE.

Samuel et al. (2025) showed that this MSE deficit over the Eastern Amazon can be amplified by plant physiology responses reducing evapotranspiration rates thereby diminishing atmospheric water content. The delay means that when onset finally does begin the season is warmer, with greater solar forcing and higher MSE values in general supporting more vigorous convective rainfall and attendant monsoonal circulations. None of the models analysed here include projected changes in land use and land cover, suggesting our results may under-estimate true magnitude of the risk of future wet season delays. The importance of the "moisture pump" provided by rainforests for supporting the transition season is well-established (Wright et al. 2017), and warmer dry seasons with higher CO_2 concentrations may reduce the effectiveness of this pump (e.g Samuel et al. 2025). Furthermore, recent studies (Smith et al. 2023b,a) quantified the impact of deforestation of pan-tropical rain forests, including the Amazon and Congo Basin. Using observational data, they reported a dry season warming of 0.018°C per percentage point of deforestation and a significant decrease in the precipitation rate during the dry and transition seasons. The loss of native Cerrado vegetation – a type of savannah typical across EBr – results in a drier and warmer transition season, effectively delaying the agricultural rainy season by 36 days (Leite-Filho et al. 2024). These results suggest that land-use change is already affecting the precipitation cycle over the region and may compound projected changes in DWTP characteristics reported here. Emerging high-resolution climate change simulations that take into account land-use change (Yoon & Hohenegger 2025) will help understand the interplay between increased atmospheric temperature, vegetation loss, and changes in the water cycle, in particular during the DWTP.

In terms of large-scale dynamics which may be driving delays in onset reported here, Chadwick et al. (2025) showed that uniform and pattern SST warming drives much of the projected SON drying over South America, with as much as 50% of the intermodel diversity in projected spring drying related to differences in South Atlantic SST warming patterns. Interactions between large-scale dynamical changes and regional thermodynamic changes are also evident in regional weather systems which support early season rainfall. Across SAfr, spring drying is associated with delays in the breakdown of the Congo Air Boundary (Howard & Washington 2020). Tropical-extratropical cloud bands driven by synoptic-scale Rossby waves (Hart et al. 2010) help support this breakdown (Howard & Washington 2019, Knight & Washington 2024) and are projected to decline significantly (Hart et al. 2026). An equivalent spring decline in tropical-extratropical cloud bands has also been documented over South America (Zilli et al. 2025).

Managing the risk posed by onset delays combined with emerging trends in early season heat waves (e.g. Ivanovich et al. 2025, Marengo et al. 2024), requires improvements to current onset early warning systems. In this context, the DWTP framework could add value to operational forecasts by diagnosing in more details the character of the transition into the wet season in a given year. Also, since the identification of the DWTP does not rely on absolute thresholds, the framework can be directly implemented in seasonal-to-subseasonal forecast systems without the need for prior bias correction. Directly diagnosing the timing of the first rains, onset intensity, fraction of dry days and other properties such as hot days, can extract information closer to the experience of farmers, water resource managers, and disaster services. Extending the DWTP metrics to other aspects such as temperature, evapotranspiration, and soil moisture could further support key decision-relevant climate services. Analysing soil moisture evolution during this transition is already underway.

6. Conclusions

This study has proposed a novel approach to flexibly identify the dry-to-wet season transition, expanding on existing methods by capturing the transitional nature of the onset season. The method reiterates existing findings warning of projected delays in rainfall onset across South America and southern Africa, using a suite of climate models including continent-wide convection-permitting regional simulations.

Because this DWTP method considers a transition, rather than a single date, based directly on rainfall rather than rain anomaly, important additional future changes to onset are uncovered. Projected delays in accumulated rainfall anomaly onset dates (Bombardi & Boos 2021, Dunning et al. 2018) could be due to lower early season rain rates and/or extension of the dry season. The DWTP directly identifies the first substantial rains or wet spell which ends the dry season and results presented here resolve the previous ambiguity to show that extended dry seasons are projected. Across South America and southern Africa, these projected delayed first rains were also shown to be followed by more intense onset periods in which the wet seasons are projected to establish more abruptly than in present climate. These changes appear consistent with dry-to-wet season thermodynamic changes already documented in existing literature.

In conclusion, the DWTP demonstrated in this paper overcomes limitations of existing methods to identify local rainfall onset and has potential to diagnose valuable metrics for observational studies, future climate studies, and emerging efforts to improve onset early warning systems.

Data availability Statement

The Unified Model data analysed during the current study are available from the corresponding author upon reasonable request.

Acknowledgments

This work was funded by First Rains, a UKRI Future Leaders Fellowship (MR/W011379/1, PI: NCGH) and through the Climate Science for Service Partnership Brazil (CSSP-Brazil) Project provided by the Met Office (UK) on behalf of the Department of Science, Innovation, and Technology (DSIT) of the UK government.

Author contributions

Marcia Zilli: Conceptualization (equal); methodology (equal); software (lead); formal analysis (lead); writing – original draft (lead). Jerry Samuel: Conceptualization (equal); methodology (equal); software (supporting); formal analysis (supporting); writing – original draft (supporting). Neil C. G. Hart: Conceptualization (equal); methodology (equal); software (supporting); formal analysis (supporting); writing – original draft (supporting); funding acquisition (lead). Francesca Morris: Conceptualization (equal); methodology (equal); software (supporting); formal analysis (supporting); writing – original draft (supporting).

References

Andrews, M. B., Ridley, J. K., Wood, R. A., Andrews, T., Blockley, E. W., Booth, B., Burke, E., Dittus, A. J., Florek, P., Gray, L. J., Haddad, S., Hardiman, S. C., Hermanson, L., Hodson, D., Hogan, E., Jones, G. S., Knight, J. R., Kuhlbrodt, T., Misios, S., Mizielinski, M. S., Ringer, M. A., Robson, J. & Sutton, R. T. (2020), 'Historical Simulations With HadGEM3-GC3.1 for CMIP6', *Journal of Advances in Modeling Earth Systems* **12**(6), 1–34. doi: 10.1029/2019MS001995.

Bombardi, R. J. & Boos, W. R. (2021), 'Explaining globally inhomogeneous future changes in monsoons using simple moist energy diagnostics', *Journal of Climate* **34**, 8615–8634. doi: 10.1175/JCLI-D-20-1012.1.

Bombardi, R. J. & Carvalho, L. M. V. (2009), 'IPCC global coupled model simulations of the South America monsoon system', *Climate Dynamics* **33**, 893–916. doi: 10.1007/s00382-008-0488-1.

URL: *http://link.springer.com/10.1007/s00382-008-0488-1*

Bombardi, R. J., Kinter, J. L. & Frauenfeld, O. W. (2019), 'A global gridded dataset of the characteristics of the rainy and dry seasons', *Bulletin of the American Meteorological Society* **100**, 1315–1328. doi: 10.1175/BAMS-D-18-0177.1.

Bony, S., Colman, R., Kattsov, V. M., Allan, R. P., Bretherton, C. S., Dufresne, J.-L., Hall, A., Hallegatte, S., Holland, M. M., Ingram, W., Randall, D. A., Soden, B. J., Tselioudis, G. & Webb, M. J. (2006), 'How well do we understand and evaluate climate change feedback processes?', *Journal of Climate* **19**, 3445–3482. doi: 10.1175/JCLI3819.1.

Carvalho, L. M. V. & Cavalcanti, I. F. A. (2016), The South American Monsoon System (SAMS), *in* L. M. Carvalho & C. Jones, eds, 'The Monsoons and Climate Change', pp. 121–148. doi: 10.1007/978-3-319-21650-8_6.

Carvalho, L. M. V., Jones, C. & Liebmann, B. (2004), 'The South Atlantic Convergence Zone: Intensity, Form, Persistence, and Relationships with Intraseasonal to Interannual Activity and Extreme Rainfall', *Journal of Climate* **17**, 88–108. doi: 10.1175/1520-0442(2004)017<0088:TSACZI>2.0.CO;2.

Chadwick, R., Good, P., Garcia-Franco, J. L., Alves, L. M., Hart, N., Zilli, M. T., Douville, H., Saint-Lu, M. & Medeiros, B. (2025), 'Processes Controlling the South American Monsoon Response to Climate Change', *Journal of Climate* **39**, 261–280. doi: 10.1175/JCLI-D-25-0012.1.

da Silva, A. E. & Carvalho, L. M. V. (2007), 'Large-scale index for South America Monsoon (LISAM)', *Atmospheric Science Letters* **8**, 51–57. doi: 10.1002/asl.150.

Dunning, C. M., Black, E. & Allan, R. P. (2018), 'Later wet seasons with more intense rainfall over Africa under future climate change', *Journal of Climate* **31**, 9719–9738. doi: 10.1175/JCLI-D-18-0102.1.

Dunning, C. M., Black, E. C. L. & Allan, R. P. (2016), 'The onset and cessation of seasonal rainfall over Africa', *Journal of Geophysical Research: Atmospheres* **121**. doi: 10.1002/2016JD025428.

Espinoza, J.-C., Jimenez, J. C., Marengo, J. A., Schongart, J., Ronchail, J., Lavado-Casimiro, W. & Ribeiro, J. V. M. (2024), 'The new record of drought and warmth in the Amazon in 2023 related to regional and global climatic features', *Scientific Reports* **14**, 8107. doi: 10.1038/s41598-024-58782-5.

FEWS-NET (2025), 'Southern Africa Seasonal Monitor-January 2025'. Available at: https://fews.net/southern-africa/seasonal-monitor/january-2025.

Fitzpatrick, R. G. J., Bain, C. L., Knippertz, P., Marsham, J. H. & Parker, D. J. (2015), 'The West African Monsoon onset: A concise comparison of definitions', *Journal of Climate* **28**, 8673–8694. doi: 10.1175/JCLI-D-15-0265.1.

Fu, R., Yin, L., Li, W., Arias, P. A., Dickinson, R. E., Huang, L., Chakraborty, S., Fernandes, K., Liebmann, B., Fisher, R. & Myneni, R. B. (2013), 'Increased dry-season length over southern Amazonia in recent decades and its implication for future climate projection', *Proceedings of the National Academy of Sciences* **110**, 18110–18115. doi: 10.1073/pnas.1302584110.

Fu, R., Zhu, B. & Dickinson, R. E. (1999), 'How Do Atmosphere and Land Surface Influence Seasonal Changes of Convection in the Tropical Amazon?', *Journal of*

Climate **12**(5), 1306–1321. doi: 10.1175/1520-0442(1999)012<1306:HDAALS>2.0.CO;2.

Funk, C., Peterson, P., Landsfeld, M., Pedreros, D., Verdin, J., Shukla, S., Husak, G., Rowland, J., Harrison, L., Hoell, A. & Michaelsen, J. (2015), 'The climate hazards infrared precipitation with stations - A new environmental record for monitoring extremes', *Scientific Data* **2**, 1–21. doi: 10.1038/sdata.2015.66.

Gan, M. A., Kousky, V. E. & Ropelewski, C. F. (2004), 'The South America Monsoon circulation and its relationship to rainfall over west-central Brazil', *Journal of Climate* **17**, 47–66. doi: 10.1175/1520-0442(2004)017<0047:TSAMCA>2.0.CO;2.

Gan, M. A., Rao, V. B. & Moscati, M. C. L. (2005), 'South American monsoon indices', *Atmospheric Science Letters* **6**, 219–223. doi: 10.1002/asl.119.

Garcia-Carreras, L., Challinor, A. J., Parkes, B. J., Birch, C. E., Nicklin, K. J. & Parker, D. J. (2015), 'The Impact of Parameterized Convection on the Simulation of Crop Processes', *Journal of Applied Meteorology and Climatology* **54**, 1283–1296. doi: 10.1175/JAMC-D-14-0226.1.

Garreaud, R. (2013), 'Warm winter storms in central chile', *Journal of Hydrometeorology* **14**, 1515–1534. doi: 10.1175/JHM-D-12-0135.1.

Gilmour, H., Chadwick, R., Catto, J. L., Halladay, K., Hart, N. C. G. & Rehbein, A. (2025), 'Mesoscale Convective Systems over South America: Representation in Kilometer-Scale Met Office Unified Model Climate Simulations', *Journal of Climate* **39**, 225–247. doi: 10.1175/JCLI-D-24-0754.1.

Halladay, K., Kahana, R., Johnson, B., Still, C., Fosser, G. & Alves, L. (2023), 'Convection-permitting climate simulations for South America with the Met Office Unified Model', *Climate Dynamics 2023* **1**, 1–23. doi: 10.1007/S00382-023-06853-0.

Hart, N. C. G., Reason, C. J. C. & Fauchereau, N. (2010), 'Tropical–Extratropical Interactions over Southern Africa: Three Cases of Heavy Summer Season Rainfall', *Monthly Weather Review* **138**, 2608–2623. doi: `10.1175/2010mwr3070.1`.

Hart, N. C. G., Reason, C. J. C. & Fauchereau, N. (2013), 'Cloud bands over southern {A}frica: seasonality, contribution to rainfall variability and modulation by the {MJO}', *Clim. Dyn.* **41**(5-6), 1199–1212.

Hart, N. C. G., Washington, R. & Maidment, R. I. (2019), 'Deep convection over Africa: Annual cycle, ENSO, and trends in the hotspots', *Journal of Climate* **32**, 8791–8811. doi: `10.1175/JCLI-D-19-0274.1`.

Hart, N. C. G., Washington, R. & Stratton, R. A. (2018), 'Stronger local overturning in convective-permitting regional climate model improves simulation of the subtropical annual cycle', *Geophysical Research Letters* **45**, 11,334–11,342. doi: `10.1029/2018GL079563`.

Hart, N., James, R., Zilli, M., Washington, R., Samuel, J. & Morris, F. (2026), The decline in tropical-extratropical cloud bands and the delay of the southern African monsoon., Technical Report EGU26-21332, Copernicus Meetings. doi: `10.5194/egusphere-egu26-21332`.
URL: *https://meetingorganizer.copernicus.org/EGU26/EGU26-21332.html*

Hersbach, H., Bell, B., Berrisford, P., Hirahara, S., Horányi, A., noz-Sabater, J. M., Nicolas, J., Peubey, C., Radu, R., Schepers, D., Simmons, A., Soci, C., Abdalla, S., Abellan, X., Balsamo, G., Bechtold, P., Biavati, G., Bidlot, J., Bonavita, M., Chiara, G., Dahlgren, P., Dee, D., Diamantakis, M., Dragani, R., Flemming, J., Forbes, R., Fuentes, M., Geer, A., Haimberger, L., Healy, S., Hogan, R. J., Hólm, E., Janisková, M., Keeley, S., Laloyaux, P., Lopez, P., Lupu, C., Radnoti, G., Rosnay, P., Rozum, I., Vamborg, F., Villaume, S. & Thépaut, J.-N. (2020), 'The ERA5 global reanalysis', *Quarterly Journal of the Royal Meteorological Society* **146**, 1999–2049. doi: 10.1002/qj.3803.

Horel, J. D., Hahmann, A. N. & Geisler, J. E. (1989), 'An investigation of the annual cycle of convective activity over the tropical Americas', *Journal of Climate* **2**, 1388–1403. doi: 10.1175/1520-0442(1989)002<1388:AIOTAC>2.0.CO;2.

Howard, E. & Washington, R. (2019), 'Drylines in southern Africa: Rediscovering the Congo air boundary', *Journal of Climate* **32**, 8223–8242. doi: 10.1175/JCLI-D-19-0437.1.

Howard, E. & Washington, R. (2020), 'Tracing Future Spring and Summer Drying in Southern Africa to Tropical Lows and the Congo Air Boundary', *Journal of Climate* **33**(14), 6205–6228. doi: 10.1175/JCLI-D-19-0755.1.

Ivanovich, C. C., Sobel, A. H., Horton, R. M., Nunes, A. M. B., da Rocha, R. P. & Camargo, S. J. (2025), 'Physical drivers of the November 2023 heatwave in Rio de Janeiro', *Weather and Climate Dynamics* pp. 1857–1874. doi: 10.5194/wcd-6-1857-2025.

Janowiak, J. E. & Xie, P. (2003), 'A global-scale examination of monsoon-related precipitation', *Journal of Climate* **16**, 4121–4133. doi: 10.1175/1520-0442(2003)016<4121:AGEOMP>2.0.CO;2.

Jones, C. & Carvalho, L. M. V. (2013), 'Climate Change in the South American Monsoon System: Present Climate and CMIP5 Projections', *Journal of Climate* **26**(17), 6660–6678. doi: 10.1175/JCLI-D-12-00412.1.

Kahana, R., Halladay, K., Alves, L. M., Chadwick, R. & Hartley, A. J. (2024), 'Future precipitation projections for Brazil and tropical South America from a convection-permitting climate simulation', *Frontiers in Climate* **6**. doi: 10.3389/fclim.2024.1419704.

Kendon, E. J., Ban, N., Roberts, N. M., Fowler, H. J., Roberts, M. J., Chan, S. C., Evans, J. P., Fosser, G. & Wilkinson, J. M. (2017), 'Do convection-permitting regional climate models improve projections of future precipitation change?', *Bulletin of the American Meteorological Society* **98**, 79–93. doi: `10.1175/BAMS-D-15-0004.1`.

Kendon, E. J., Stratton, R. A., Tucker, S., Marsham, J. H., Berthou, S., Rowell, D. P. & Senior, C. A. (2019), 'Enhanced future changes in wet and dry extremes over Africa at convection-permitting scale', *Nature Communications* **10**, 1794. doi: `10.1038/s41467-019-09776-9`.

Knight, C. & Washington, R. (2024), 'Remote midlatitude control of rainfall onset at the southern African tropical edge', *Journal of Climate* **37**, 2519–2539. doi: `10.1175/JCLI-D-23-0446.1`.

Kodama, Y. (1992), 'Large-scale common features of subtropical precipitation zones (the Baiu Frontal Zone, the SPCZ, and the SACZ) Part I: Characteristics of subtropical frontal zones', *Journal of the Meteorological Society of Japan. Ser. II* **70**, 813–836. doi: `10.2151/jmsj1965.70.4_813`.

Kousky, V. E. (1988), 'Pentad outgoing longwave radiation climatology for the South American sector', *Revista Brasileira de Meteorologia* **3**, 217–231. Available at: `https://citeseerx.ist.psu.edu/document?repid=rep1&type=pdf&doi=4116acd118c931e3869e91d38a4d3cd04f7bfeb6`.

Kuhlbrodt, T., Jones, C. G., Sellar, A., Storkey, D., Blockley, E., Stringer, M., Hill, R., Graham, T., Ridley, J., Blaker, A., Calvert, D., Copsey, D., Ellis, R., Hewitt, H., Hyder, P., Ineson, S., Mulcahy, J., Siahaan, A. & Walton, J. (2018), 'The Low-Resolution Version of HadGEM3 GC3.1: Development and Evaluation for Global Climate', *Journal of Advances in Modeling Earth Systems* **10**(11), 2865–2888. doi: `10.1029/2018MS001370`.

Lawal, S., Hewitson, B. & Lennard, C. (2024), 'Assessing the Climatological Characteristics of Observed and Simulated Seasonal Onset of Precipitation Over Southern and Eastern Africa', *International Journal of Climatology* **44**(16), 5791–5808. doi: 10.1002/joc.8666.

Leite-Filho, A. T., Soares-Filho, B. S., Oliveira, U. & Coe, M. (2024), 'Intensification of climate change impacts on agriculture in the cerrado due to deforestation', *Nature Sustainability* **8**, 34–43. doi: 10.1038/s41893-024-01475-8.

Lenderink, G., Ban, N., Brisson, E., Berthou, S., Cortés-Hernández, V. E., Kendon, E., Fowler, H. & de Vries, H. (2024), 'Are dependencies of extreme rainfall on humidity more reliable in convection-permitting climate models?', *Hydrology and Earth System Sciences Discussions* pp. 1–31. doi: 10.5194/hess-2024-132.

Li, W. & Fu, R. (2004), 'Transition of the Large-Scale Atmospheric and Land Surface Conditions from the Dry to the Wet Season over Amazonia as Diagnosed by the ECMWF Re-Analysis', *Journal of Climate* **17**(13), 2637–2651. doi: 10.1175/1520-0442(2004)017<2637:TOTLAA>2.0.CO;2.

Liebmann, B., Bladé, I., Kiladis, G. N., Carvalho, L. M. V., Senay, G. B., Allured, D., Leroux, S. & Funk, C. (2012), 'Seasonality of African precipitation from 1996 to 2009', *Journal of Climate* **25**, 4304–4322. doi: 10.1175/JCLI-D-11-00157.1.

Liebmann, B. & Marengo, J. (2001), 'Interannual variability of the rainy season and rainfall in the Brazilian Amazon Basin', *Journal of Climate* **14**, 4308–4318. doi: 10.1175/1520-0442(2001)014<4308:IVOTRS>2.0.CO;2.

Marengo, J. A., Cunha, A. P., Espinoza, J.-C., Fu, R., Schöngart, J., Jimenez, J. C., Costa, M. C., Ribeiro, J. M., Wongchuig, S. & Zhao, S. (2024), 'The drought of Amazonia in 2023-2024', *American Journal of Climate Change* **13**, 567–597. doi: 10.4236/ajcc.2024.133026.

Marengo, J. A., Liebmann, B., Kousky, V. E., Filizola, N. P. & Wainer, I. C. (2001), 'Onset and End of the Rainy Season in the Brazilian Amazon Basin', *Journal of Climate* **14**, 833–852. doi: 10.1175/1520-0442(2001)014<0833:OAEOTR>2.0.CO;2.

Mattingly, K. S. & Mote, T. L. (2017), 'Variability in warm-season atmospheric circulation and precipitation patterns over subtropical South America: relationships between the South Atlantic Convergence Zone and large-scale organized convection over the La Plata basin', *Climate Dynamics* **48**, 241–263. doi: 10.1007/s00382-016-3072-0.

Munday, C., Washington, R., Engelstaedter, S., Zilli, M., Harbord, S., Knight, C., Attwood, K. & Hart, N. (2025), 'Southern African climate change: Processes, models, and projections', *WIREs Climate Change* **16**. doi: 10.1002/wcc.70025.

Mwangi, E., MacLeod, D., Kniveton, D. & Todd, M. C. (2024), 'Variability of rainy season onsets over East Africa', *International Journal of Climatology* **44**(10), 3357–3379. doi: 10.1002/joc.8528.

Nieto-Ferreira, R. & Rickenbach, T. M. (2011), 'Regionality of monsoon onset in South America: a three-stage conceptual model', *International Journal of Climatology* **31**, 1309–1321. doi: 10.1002/joc.2161.

Raia, A. & Cavalcanti, I. F. A. (2008), 'The life cycle of the South American Monsoon System', *Journal of Climate* **21**, 6227–6246. doi: 10.1175/2008JCLI2249.1.

Reason, C. J. C., Hachigonta, S. & Phaladi, R. F. (2005), 'Interannual variability in rainy season characteristics over the Limpopo region of Southern Africa', *International Journal of Climatology* **25**, 1835–1853. doi: 10.1002/joc.1228.

Reynolds, R. W., Smith, T. M., Liu, C., Chelton, D. B., Casey, K. S. & Schlax, M. G. (2007), 'Daily High-Resolution-Blended Analyses for Sea Surface Temperature', *Journal of Climate* **20**(22), 5473–5496. doi: 10.1175/2007JCLI1824.1.

Samuel, J. B., Zilli, M. T., Hart, N. C. G., Halladay, K., Kahana, R., Chadwick, R. & Folwell, S. (2025), 'Simulated delay in the onset of the rainy season in Central-East Brazil under global warming influenced by plant physiological response', *Journal of Climate* **38**, 6853–6872. doi: 10.1175/JCLI-D-24-0720.1.

Smith, C., Baker, J. C. A. & Spracklen, D. V. (2023b), 'Tropical deforestation causes large reductions in observed precipitation', *Nature* **615**, 270–275. doi: 10.1038/s41586-022-05690-1.

Smith, C., Robertson, E., Chadwick, R., Kelley, D. I., Argles, A. P. K., Coelho, C. A. S., de Souza, D. C., Kubota, P. Y., Talamoni, I. L., Spracklen, D. V. & Baker, J. C. A. (2023a), 'Observed and simulated local climate responses to tropical deforestation', *Environmental Research Letters* **18**, 104004. doi: 10.1088/1748-9326/acf0da.

Stratton, R. A., Senior, C. A., Vosper, S. B., Folwell, S. S., Boutle, I. A., Earnshaw, P. D., Kendon, E., Lock, A. P., Malcolm, A., Manners, J., Morcrette, C. J., Short, C., Stirling, A. J., Taylor, C. M., Tucker, S., Webster, S. & Wilkinson, J. M. (2018), 'A Pan-African convection-permitting regional climate simulation with the met office unified model: CP4-Africa', *Journal of Climate* **31**, 3485–3508. doi: 10.1175/JCLI-D-17-0503.1.

Stríkis, N. M., Buarque, P. F. S. M., Cruz, F. W., Bernal, J. P., Vuille, M., Tejedor, E., Santos, M. S., Shimizu, M. H., Ampuero, A., Du, W., Sampaio, G., dos Reis Sales, H., Campos, J. L., Kayano, M. T., Apaèstegui, J., Fu, R. R., Cheng, H., Edwards, R. L., Mayta, V. C., da Silva Francischini, D., Arruda, M. A. Z. & Novello, V. F. (2024), 'Modern anthropogenic drought in central Brazil unprecedented during last 700 years', *Nature Communications* **15**, 1728. doi: 10.1038/s41467-024-45469-8.

Tadross, M. A., Hewitson, B. C. & Usman, M. T. (2005), 'The interannual variability of the onset of the maize growing season over South Africa and Zimbabwe', *Journal* *of Climate* **18**, 3356–3372. doi: 10.1175/JCLI3423.1.

Thoithi, W., Blamey, R. C. & Reason, C. J. C. (2021), 'Dry Spells, Wet Days, and Their Trends Across Southern Africa During the Summer Rainy Season', *Geophysical Research Letters* **48**(5), e2020GL091041. doi: 10.1029/2020GL091041.

Williams, K. D., Copsey, D., Blockley, E. W., Bodas-Salcedo, A., Calvert, D., Comer, R., Davis, P., Graham, T., Hewitt, H. T., Hill, R., Hyder, P., Ineson, S., Johns, T. C., Keen, A. B., Lee, R. W., Megann, A., Milton, S. F., Rae, J. G. L., Roberts, M. J., Scaife, A. A., Schiemann, R., Storkey, D., Thorpe, L., Watterson, I. G., Walters, D. N., West, A., Wood, R. A., Woollings, T. & Xavier, P. K. (2018), 'The Met Office Global Coupled Model 3.0 and 3.1 (GC3.0 and GC3.1) Configurations', *Journal of Advances in Modeling Earth Systems* **10**(2), 357–380. doi: 10.1002/2017MS001115.

Wright, J. S., Fu, R., Worden, J. R., Chakraborty, S., Clinton, N. E., Risi, C., Sun, Y. & Yin, L. (2017), 'Rainforest-initiated wet season onset over the southern Amazon', *Proceedings of the National Academy of Sciences of the United States of America* **114**(32), 8481–8486. doi: 10.1073/pnas.1621516114.

Yoon, A. & Hohenegger, C. (2025), 'Muted amazon rainfall response to deforestation in a global storm-resolving model', *Geophysical Research Letters* **52**. doi: 10.1029/2024GL110503.

Zilli, M. T., Hart, N. C. G., Halladay, K. & Kahana, R. (2025), 'Threefold increase in most intense South Atlantic convergence zone events by 2100 in convection-permitting simulation', *Environmental Research Letters* **20**, 074045. doi: 10.1088/1748-9326/ade16e.

Zilli, M. T., Lemes, M. R., Hart, N. C. G., Halladay, K., Kahana, R., Fisch, G., Prein, A., Ikeda, K. & Liu, C. (2024), 'The added value of using convective-permitting regional

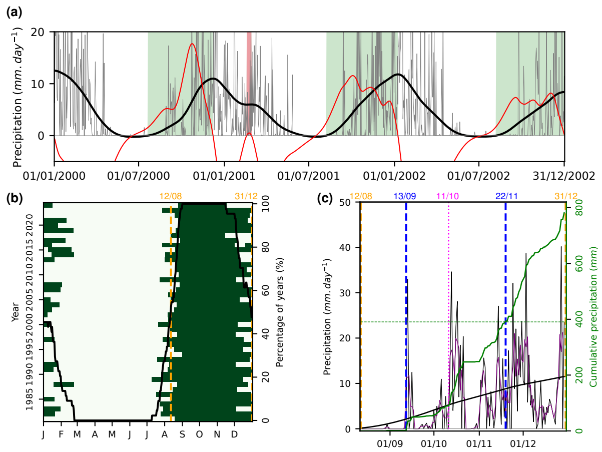

Graphical Abstract: Graphics exemplifying the main steps of the DWTP framework: (a) Identification of the periods with positive filtered precipitation and its gradient. (b) Definition of the climatological envelope. (c) refinement of the DWTP for a given year.

climate model simulations to represent cloud band events over South America', *Climate Dynamics* **62**, 10543–10564. doi: 10.1007/s00382-024-07460-3.

Graphical Abstract

We introduce a novel framework to identify the Dry-to-Wet Transition Period (DWTP), capturing the transition from the first significant rainfall to the establishment of sustained wet-season conditions. Applied to South America and Southern Africa, the framework provides novel insights to the transition period complementing the conventional single-date methodologies. Climate projections indicate a delayed, shorter, and more abrupt transition. The DWTP provides a flexible tool for climate assessment, seasonal forecasting, and early warning systems.